

Article

Amplification of Extreme Hot Temperatures over Recent Decades

Nir Y. Krakauer ^{1,2} 

¹ Department of Civil Engineering and NOAA-CESSRST, City College of New York, New York, NY 10031, USA; mail@nirkrakauer.net

² Earth and Environmental Sciences, City University of New York Graduate Center, New York, NY 10017, USA

Abstract: While global warming is mostly conceptualized in terms of increases in mean temperature, changes in the most extreme conditions encountered often have disproportionate impacts. Here, a measure of warming amplification is defined as the change in the highest yearly temperature (denoted TXx), representing extreme heat, minus that in the 80th percentile daily high temperature (T_{\max}^{80}), which represents typical summer conditions. Based on the ERA5 reanalysis, over 1959–2021, warming of TXx averaged 1.56 K over land areas, whereas warming of T_{\max}^{80} averaged 1.60 K. However, the population-weighted mean warming of TXx significantly exceeded warming of T_{\max}^{80} (implying positive amplification) over Africa, South America, and Oceania. Where available, station temperature observations generally showed similar trends to ERA5. These findings provide a new target for climate model calibration and insight for evaluating the changing risk of temperature extremes.

Keywords: climate change; climate extremes; heat stress

1. Introduction

Global warming is mostly conceptualized in terms of increases in mean temperature. However, changes in the most extreme weather conditions encountered, which can be thought of as deriving from a shift in the variance and other moments of the temperature probability distribution in addition to an increase in its mean, often has disproportionate impacts [1–4]. For example, extremely high temperatures are particularly likely to harm organisms and ecosystems, including direct heat impacts on human health, as well as strain infrastructure such as electricity and water delivery systems. Therefore, it is important to study the change in propensity for temperature extremes as compared to the warming of mean or typical conditions, and how this might differ between regions.

Previous work on this topic has resulted in the definition of a suite of indices of change in extreme temperature, as well as in other weather extremes [5,6], now as part of the World Climate Research Programme Grand Challenge on Weather and Climate Extremes [7]. Datasets have been generated of changes in extreme temperatures over time based on either station records, reanalyses, global climate models, or satellite remote sensing [8–14]. Changes in extreme temperatures have been studied in the context of increased risk of heat waves, for example in agricultural regions and urban areas [15–18]. One source of variability may be associated with irrigated areas, for which agricultural intensification may be suppressing hot temperature extremes through promoting high evapotranspiration rates during the growing season [19–22].

The latest Intergovernmental Panel on Climate Change (IPCC) report on the physical science of climate change presents the current understanding of climate change impacts on different weather and climate extremes in a chapter of over 200 pages [23]. Published analysis of weather station data, summarized by IPCC, finds that annual maximum temperature (TXx), a commonly used indicator of extreme heat, has been on average warming at about the same rate as annual mean temperature [24,25]. However, no systematic global study



Citation: Krakauer, N.Y.

Amplification of Extreme Hot

Temperatures over Recent Decades.

Climate **2023**, *11*, 42. <https://doi.org/10.3390/cli11020042>

Academic Editor: Mário Gonzalez

Pereira

Received: 4 January 2023

Revised: 30 January 2023

Accepted: 7 February 2023

Published: 10 February 2023



Copyright: © 2023 by the authors.

Licensee MDPI, Basel, Switzerland.

This article is an open access article distributed under the terms and conditions of the Creative Commons Attribution (CC BY) license (<https://creativecommons.org/licenses/by/4.0/>).

is reported of the spatial distribution of any differences between the mean and extreme temperature trends.

Whether extremely hot temperatures are increasing faster or slower than mean temperatures at a particular location could be important for evaluating impacts that are particularly tied to extreme heat, and could also suggest which processes differentially affect extreme heat and need to be modeled in order to accurately project future changes. The current study aims to help fill this gap by considering warming in TXx as a measure of extreme heat versus warming in a measure of typical summer temperature across continents, using a state-of-the-art global reanalysis that is also compared with station data.

In the current study, a measure of warming amplification is defined as the change in the highest yearly temperature (TXx) minus that in the 80th percentile daily high temperature, which represents typical summer conditions. This work highlights areas where the hazard of extreme temperatures is increasing faster than would be expected based on overall heating.

2. Methods

2.1. Extreme Heat and Amplification Measure

The measure of extreme heat chosen was TXx, the highest temperature recorded each calendar year [6]. TXx was suitable because it is more extreme than other common temperature-based measures of extreme heat such as the 95th or 99th percentile, yet, with a value each year, it lent itself better to the statistical analysis of trends over periods of a few decades compared to measures such as the highest temperature in a 20 or 30 year period.

The warming of TXx was compared with that in typical summer daytime temperature, as indicated by T_{\max}^{80} , or the 80th percentile of daily maximum temperature each calendar year. This focused the analysis on warm-season anomalies, and avoided confounding by, for example, nighttime temperatures warming faster than daytime temperatures, and winter temperatures warming faster than summer temperatures [24,26].

The position of T_{\max}^{80} in the summer temperature probability distribution was checked using all 4468 weather stations in version 3.1.2.202107p of the HadISD database [27,28] that had at least 10 complete years of subdaily temperature data. Defining summer as the climatologically warmest 3 months at each station, the station T_{\max}^{80} was a median of the 38th percentile of summer maximum temperature (range across stations: 20th to 93rd percentile) and a median of the 79th percentile of temperature across all summer hours (range: 33rd to 99th). Thus, while there is variation in the mapping between percentiles of all-year daily maximum temperature and percentiles of summer temperature that relates to temperature seasonality and diurnal range, temperatures at or above T_{\max}^{80} are typically found in about 60% of summer days as the daily maximum and in about 20% of all summer hours, supporting its description as a typical summer temperature and contrast with TXx, the annual maximum.

For each year, a summer temperature range ΔT was defined as $\text{TXx} - T_{\max}^{80}$. An amplification factor A was defined as the estimated increase in ΔT between the first and last year of the study period, as determined by cubic spline smoothing of the yearly ΔT series. $A > 0$ (positive amplification) would correspond to the hottest temperatures warming faster than typical summer temperatures (or amplified warming under hot temperature extremes), while $A < 0$ (negative amplification) would imply slower warming of the hottest days (or dampened warming under extreme conditions). All smoothing cubic splines were computed using a smoothing parameter value chosen to approximately optimize the corrected Akaike information criterion [29,30] for ΔT time series of a random sample of 1000 points.

2.2. Reanalysis Data

ERA5 is the fifth-generation European Centre for Medium-Range Weather Forecasts (ECMWF) Reanalysis [31]. ERA5 assimilates large amounts of station and satellite data in order to provide a dynamically consistent representation of weather and climate that is

considered state of the art [32] and has been used for many applications, including research on heat extremes and their trends [18,33–37]. ERA5 is currently available for the period from 1959 to a few months before the present. Analyzed ERA5 fields are available hourly at a 0.25° horizontal resolution. To compute TX_x , T_{\max}^{80} , and their differences and trends for 1959–2021, the 2-m (surface) air temperature field was downloaded and the hourly values aggregated to daily maximums, using Universal Time to define days.

2.3. Station-Based Data

The ERA5 T_{\max}^{80} , TX_x , and their difference and trends were checked against the corresponding indices derived from weather station daily maximum temperature series. There are several reasons why station data are not expected to show exactly the same means and trends as a reanalysis, including the difference in spatial scale, in the definition of daily maximums (in ERA5 these are the highest hourly values, whereas stations will usually also record maximums that were reached in the middle of an hour), and likely inhomogeneities in siting or instrumentation at some stations. Nevertheless, the station values offer a valuable check on the representation of the temperature field in the reanalysis. All stations with available data were extracted from the Global Historical Climatology Network (GHCN)-Daily database [38,39]. After excluding data with quality control flags [40], only the stations with at least 40 years of complete daily data in 1959–2021 were retained. Spline smoothing was used to estimate 1959–2021 averages and trends at each location, with linear extrapolation invoked if the first or last years of the period were missing for a particular station. Each station's averages and trends were then compared with those of ERA5 sampled at the same grid cell and for the same years that had complete data, and processed with the same smoothing spline method.

2.4. Ancillary Data

In order to study changes over populated areas, the 2020 population distribution from the Gridded Population of the World (GPW) dataset (version 4.11) were downloaded at 1/24° resolution and then regridded to match the ERA5 resolution. GPW is based on national census data disaggregated to the best available administrative-unit resolution [41,42]. Area and population weighted global and continental averages were then computed as

$$\bar{T} = \frac{\sum_i w_i T_i}{\sum_i w_i},$$

where the weighting w_i is either the area or the population of each grid cell in the world or continent, T_i is the temperature quantile value for each grid cell, and \bar{T} is the resulting computed average value.

As a measure of agricultural intensification that could potentially support high transpiration levels and suppress warm temperature extremes, the grid area fraction equipped for irrigation as of circa 2005 was obtained from version 5 of the Food and Agriculture Organization's Global Map of Irrigation Areas (GMIA), regridding from its resolution of 1/12° to match the ERA5 grid. GMIA combines national censuses and reports, reports from international agencies, and interpretation of satellite photographs [43,44].

2.5. Significance Testing

As a measure of whether any trend in mean amplification A is likely to be robust to year-to-year climate variability, 95% confidence intervals for the Theil–Sen slope of the time series of yearly A at global and continental scales were estimated using the bootstrap procedure recommended by Ref. [45]. The test is for a monotonic, but not necessarily linear trend, and unlike the spline smoothing that is also used here, it is robust to individual outlying years [46].

3. Results

3.1. Mean Spatial Patterns

Typical summer daily maximum temperatures in ERA5, as summarized by T_{\max}^{80} (Figure 1a), were, as expected, highest in subtropical and desert land areas and, at a given latitude, tended to be lower over the oceans as well as at high elevations. The difference ΔT between T_{\max} and T_{\max}^{80} had a distinctive behavior (Figure 1b). While higher over land than over the oceans (mean ΔT was 7.66 °C over land compared to only 2.26 °C over water), it was not necessarily higher in the deserts, but instead peaked at the poleward margins of continents, where summer conditions are dominated by flow from the nearby mild ocean but sometimes receive much hotter continental air. For example, western Europe, which experiences occasional heat waves associated with hot and dry Saharan air masses, tended to have higher summer temperature range ΔT than the Sahara itself, which is more consistently hot in summer.

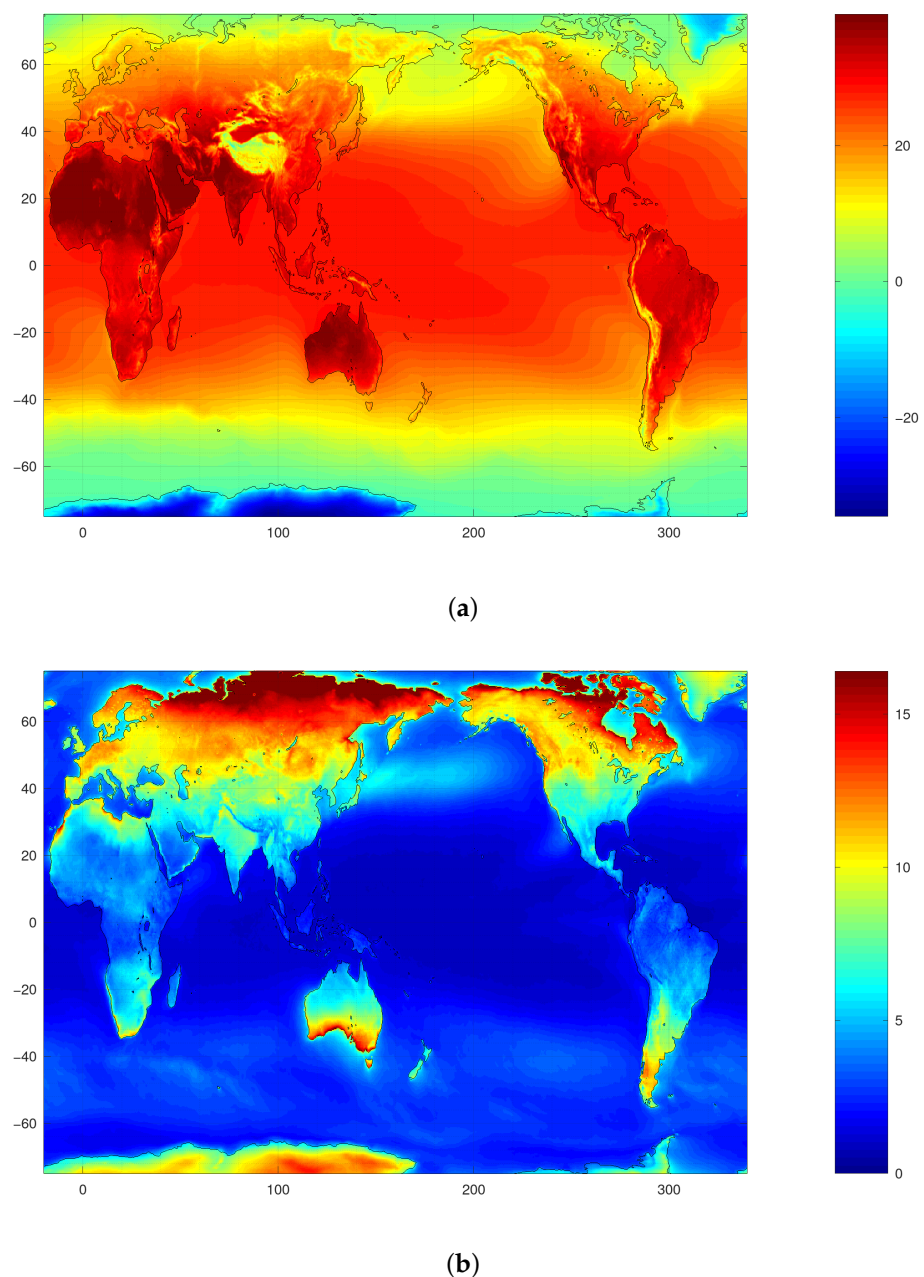


Figure 1. (a) ERA5 mean T_{\max}^{80} (°C), 1959–2021. (b) ERA5 mean difference between T_{\max} and T_{\max}^{80} (°C), 1959–2021.

3.2. Warming and Amplification

The trend in T_{\max}^{80} in ERA5 showed strong warming of 1–3 °C between 1959 and 2021 in most land regions, and warming of typically 0.5–1 °C over oceans (Figure 2a). High-latitude and desert regions tended to warm the most. Some land areas that showed little or no warming are those known to have experienced agricultural intensification and expansion of irrigated area, such as the northern Great Plains in North America and the Indus Valley [47,48], or enhanced sea breeze, such as coastal California [49,50]. ERA5 also showed less or no summer warming over the Laurentian Great Lakes, with cooling over Lake Superior, which is inconsistent with in situ and satellite data that show rapid summer warming there [51–53] and may point to problems in modeling or data assimilation over lakes in ERA5.

Meanwhile, the change A in ΔT between 1959 and 2021 in ERA5 showed pronounced local and regional differences, mostly in the range -2 to $+2$ °C (Figure 2b). For example, A was positive over much of Europe, meaning that extreme warm temperatures increased faster than mean summer temperatures, but near zero over Italy and northern Scandinavia. A was negative over some irrigated areas, such as California’s Central Valley, the USA Midwest, and the Ganges Valley, but positive over others, such as the Indus valley and the Mississippi delta.

Overall, the warming in T_{\max}^{80} between 1959 and 2021 in ERA5 averaged 1.62 °C over land and 0.71 °C over water. The amplification A averaged -0.23 °C over land and 0.10 °C over water, indicating that on average over land TXx increased more slowly than T_{\max}^{80} while over ocean it increased more quickly. However, over both land and water, there are wide variations between positive and negative values (Figure 2b).

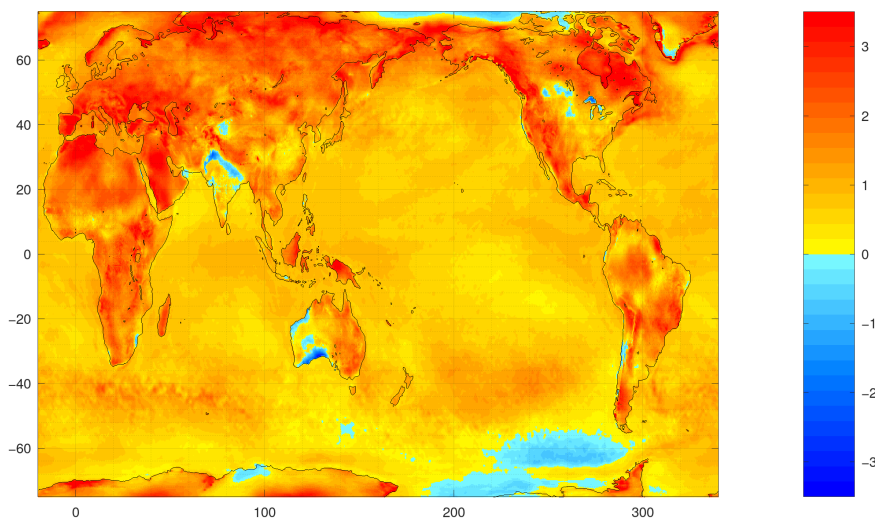
On continental scales, average A was significantly below zero over Asia and positive over Europe. When weighted by population, the average A was no longer significantly different from zero globally or over Asia and Europe, but was significantly above zero in Africa, Oceania, and South America (Table 1).

Table 1. Smoothed change in T_{\max}^{80} , TXx, and in their difference (amplification A) over 1959–2021 in ERA5 by water/land and continent.

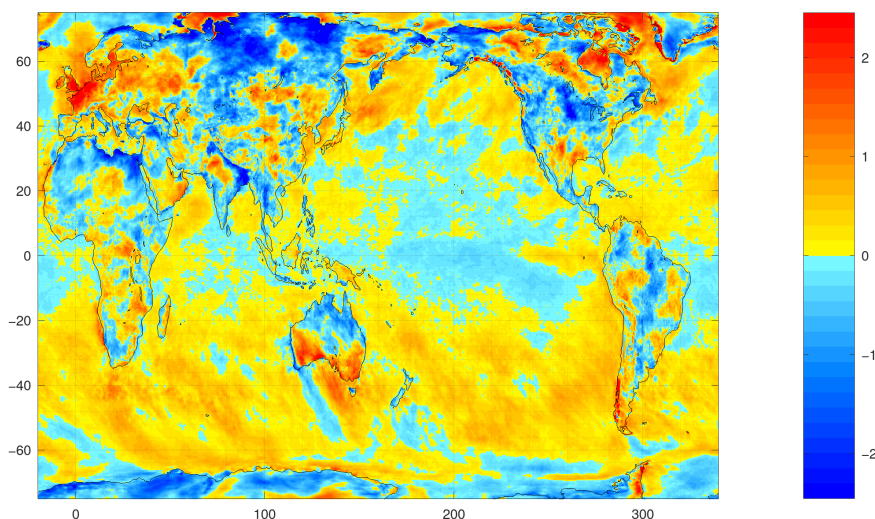
	ΔT_{\max}^{80}	ΔTXx	A
Water	0.72	0.85	0.13 *
Land	1.60 (0.82)	1.56 (0.92)	-0.04 * (0.10)
Africa	1.71 (1.90)	1.69 (2.40)	-0.02 (0.49 *)
Asia	1.68 (1.15)	1.46 (1.27)	-0.22 * (0.12)
Australia	0.01 (0.39)	1.00 (0.52)	0.99 (0.13)
North America	1.70 (1.43)	1.57 (1.92)	-0.13 (0.59)
Oceania	1.32 (0.61)	1.13 (0.72)	-0.19 (0.11 *)
South America	1.10 (1.20)	1.04 (1.44)	-0.06 (0.25 *)
Antarctica	1.34	1.30	-0.05
Europe	2.19 (1.70)	2.48 (2.14)	0.29 * (0.44)

The values in parentheses are population-weighted averages; the other values are area-weighted averages. Starred values of A are significantly different from zero at the 0.05 level (two-tailed).

Grid cells that were at least partly equipped for irrigation (17% of the land area, but accounting for 89% of world population) had only slightly lower area-average amplification than other land grid cells (-0.12 versus -0.09 °C). Moreover, for the grid cells that were at least partly equipped for irrigation, there was little correlation between the fraction equipped for irrigation and amplification (the Spearman rank correlation between the two quantities was 0.008). Thus, globally, agricultural intensification as expressed in equipment for irrigation did not appear to be a major factor in explaining spatial variability in amplification.



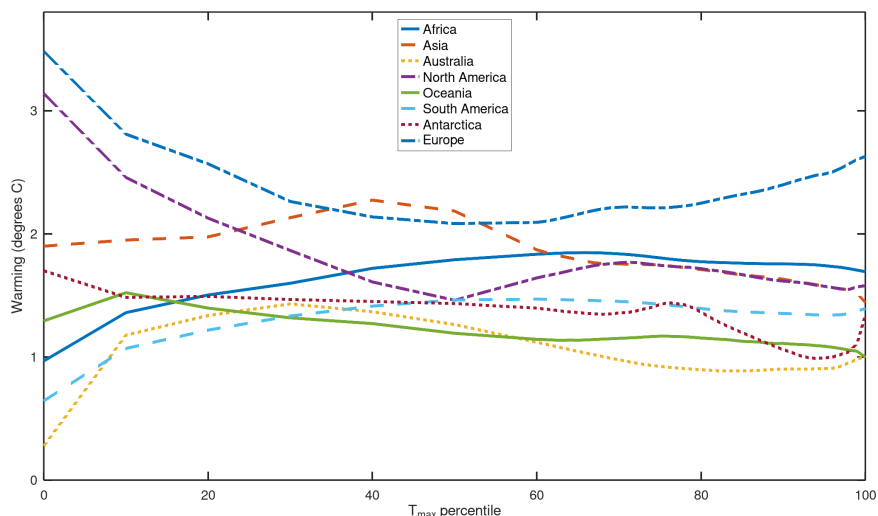
(a)



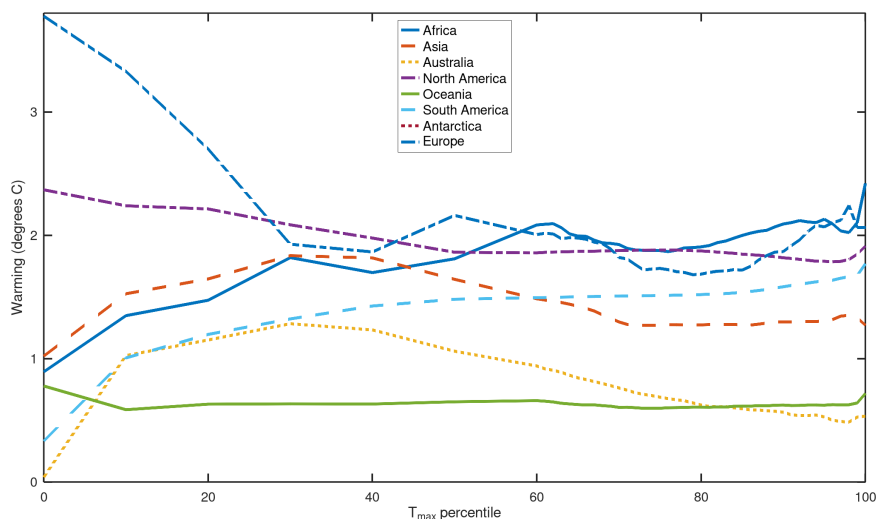
(b)

Figure 2. (a) Smoothed ERA5 change in T_{\max}^{80} (K), 1959–2021. (b) Smoothed ERA5 change in the difference between TXx and T_{\max}^{80} (K), 1959–2021.

To assess the sensitivity of the amplification quantities to the choice of T_{\max} percentiles considered compared to the 80th (T_{\max}^{80}) and 100th (TXx) chosen here, the continental warming between 1959 and 2021 in ERA5 was also plotted across T_{\max} percentiles (Figure 3). For the most part, the warming rate is a relatively smooth function of the T_{\max} percentile. The largest differences between TXx and the 99th percentile are seen in Antarctica and in Africa with population weighting, both of which have TXx warming faster than the less extreme 99th percentile. For the most part, the amplification factor would be similar if the typical summer temperature was taken as the 70th or 90th as opposed to the 80th percentile, although in Europe with population weighting, this would make A less positive (Figure 3b). The lowest percentiles, corresponding to winter conditions in the extratropics, warmed much faster than the median in Europe and North America but similar to or less than the median in other continents, similar to what was found in earlier work based on station data [26].



(a)



(b)

Figure 3. (a) Smoothed ERA5 change in different percentiles of T_{max} , 1959–2021, by continent (area-weighted average), showing every 10th percentile up to the 60th, then every percentile. The 0th percentile corresponds to the coldest T_{max} of each year and the 100th percentile to the annual maximum temperature T_{max} . (b) Same, but using population-weighted averages.

3.3. Comparison with GHCN-D Station Data

There were 2118 stations in GHCN-D with sufficiently complete daily maximum temperature data for 1959–2021. The stations were concentrated in the USA, Europe, and China, with some also in Siberia and Australia, but almost none in Africa and none in South America or the Indian subcontinent (Figure 4a). GHCN-D had somewhat larger mean ΔT than the corresponding ERA5 grid cells (9.95 vs. 9.44 °C), which is reasonable considering that a global reanalysis would miss some of the small-scale spatial and temporal variability that could drive up yearly extremes. ERA5 well captured the GHCN-D interstation variability in interannual-mean T_{max}^{80} (correlation of 0.971 between GHCN-D and subsampled ERA5) and ΔT (correlation of 0.890).

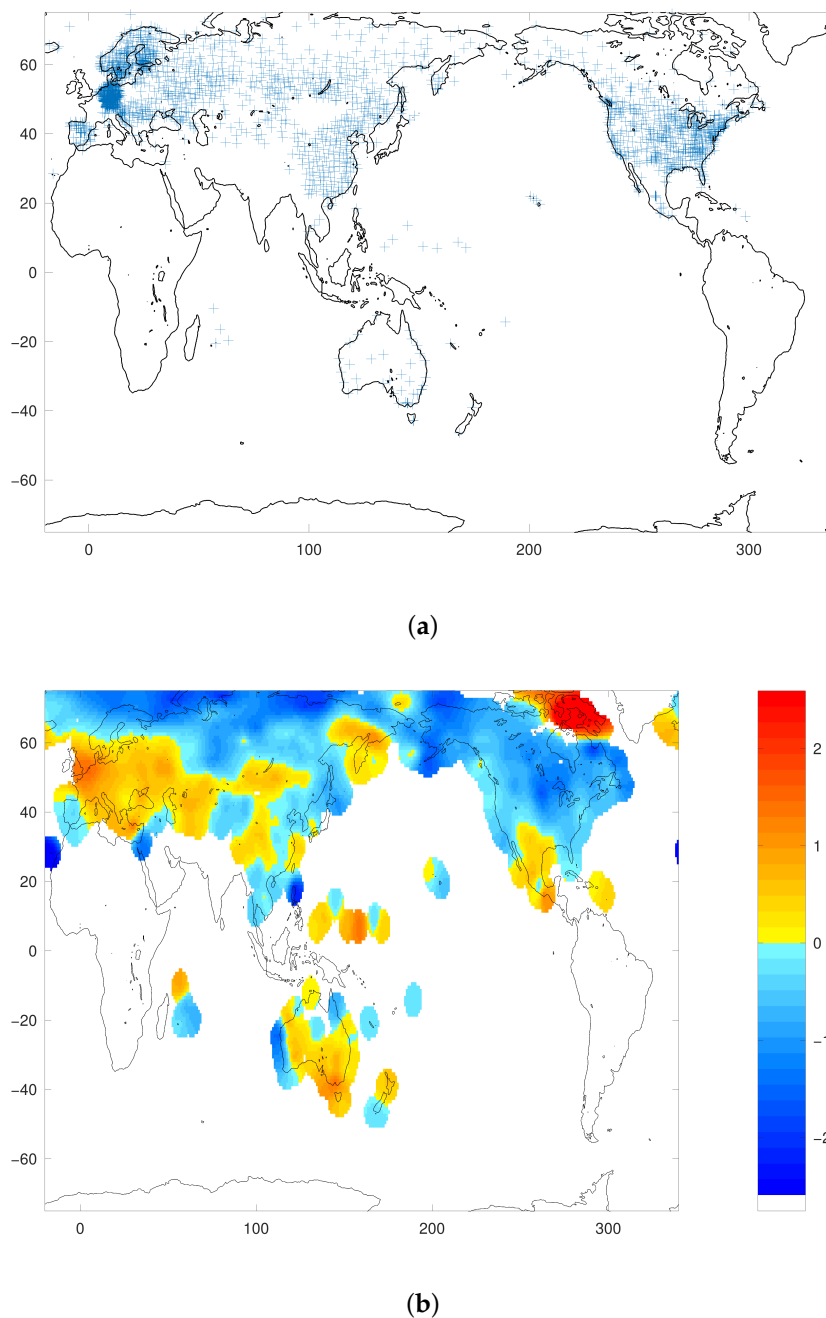


Figure 4. (a) Locations of GHCN-D stations available to compare with ERA5. (b) Change in the difference between TXx and T_{\max}^{80} (°C), 1959–2021, based on spatial interpolation of GHCN-D stations. In the interpolation scheme, station values were weighted based on distance to each interpolation point with an exponential decay length scale of 2° . Interpolation was not performed for grid points over 4° away from a GHCN-D station.

The average 1959–2021 warming in T_{\max}^{80} for the GHCN-D stations compared well with ERA5 for the same grid cells (GHCN-D: 1.65°C , ERA5: 1.67°C), although the average amplification A at station locations was somewhat more positive in the reanalysis (GHCN-D: 0.03°C , ERA5: 0.26°C). The spatial distribution of A showed a strong positive correlation of 0.763 between GHCN-D stations and ERA5, and GHCN-D showed many of the same patterns as ERA5 of, for example, regions of negative A centered over northern Siberia and the northern Great Plains of the United States, and positive A over western Europe (Figure 4b).

4. Discussion

Based on ERA5, over land in 1959–2021, annual maximum temperatures TXx warmed about 3% more slowly than 80th percentile daily maxima T_{\max}^{80} (by 1.56 versus 1.60 °C), for a negative mean amplification A (−0.04 °C). This refines the current perception in the scientific literature that the hot extremes of the temperature distribution, such as TXx, are increasing at about the same rate as its center, and that temperature variability shows no obvious trend [23,54]. A possible physical reason for a slower increase in TXx over land is the nonlinearity with temperature of thermal radiation emission, such that at higher temperatures, a given radiative forcing is balanced by a smaller temperature increase. On the other hand, over water, TXx has warmed about 18% faster than T_{\max}^{80} over the same period, for a positive mean A (0.13 °C). This could be due to the temperature range over water being characteristically much less than over land, so that the nonlinearity in thermal emission is less important, along with an increase in land-sea summer temperature contrast (as the land surface has warmed faster than the oceans) [55], such that the incursion of continental air can now lead to higher peak temperatures compared to the new over-water mean temperature. Weighting by population instead of land area, mean A was not significantly different from zero.

Along with the mean value for amplification A , there was pronounced regional variability. Some regions, including much of Europe, north-central India, the south-central United States, and inland southeast and southwest Australia, had annual maximum temperatures increasing much faster than typical summer temperatures (positive A). In other cases, such as over the Ganges basin, northeast Africa, the northern Great Plains of central North America, and much of Siberia, annual maxima have warmed much less (negative A). These regional differences can have important implications for the frequency of the most severe impacts on human and ecosystem health.

Ref. [56] found that hot days over tropical land warm more than the average day, which is attributed to a ‘drier get hotter’ mechanism. This is based on the idea that the days with the highest temperature tend to be the driest ones (with low soil moisture), and therefore less of the additional heat can go to evaporating water, compared to average days in the moist tropics. This hypothesis is consistent with the positive mean population-weighted amplification seen over primarily tropical Africa, Oceania, and South America. However, plotting mean ERA5 amplification by latitude over land (not shown) did not reveal clear overall trends. Northwest Europe could be an example of an extratropical region that normally has abundant moisture during the hot season for evaporation that keep temperatures down, but can be subject to occasional drought that dominates TXx [57–59], explaining the strongly positive A there. Over water, by contrast, where the moisture supply does not limit evaporation, the trend was towards higher amplification in the mid-latitudes, which at least in the Northern Hemisphere possibly reflects the faster warming over land there that leads to relatively hotter available continental air. Climate-mode experiments also show that the plant physiological response to rising CO₂ levels, including higher water use efficiency, tends to increase TXx over Europe while decreasing it over central North America [60], which is broadly consistent with the trends shown here.

The strengths of this study include defining an amplification metric to exclude diurnal and seasonal effects, using a state-of-the-art reanalysis with high spatial and temporal resolution, and analysis at global and continental scales. On the other hand, many factors such as topography, biome, and soil type may also affect amplification, and could be examined in future research. Land cover and land use aspects such as urbanization [15] and irrigated agriculture [61,62], as well as atmospheric forcing agents such as aerosols [63], clearly affect amplification and also need to be considered. While the correlation of amplification with an area equipped for irrigation was investigated here and found to be small overall, it may be important regionally, depending for example on the seasonality of irrigation versus that of peak temperature.

In addition, by considering only temperature as an extreme heat metric, this study left out the role of humidity in aggravating heat stress. For example, while irrigation is

modeled to mitigate hot temperature extremes, it also increases humidity and therefore potentially measures of humid heat extremes [34,37]. Moreover, amplification showed strong regional variability beyond the pattern associated with climate zones, likely due to local surface conditions and atmospheric circulation. For example, Europe, where heat extremes are associated with the flow of Saharan air from the south combined with local drought [58,64], showed particularly high amplification. Another hot spot of high A was in the southern Amazon basin, which could be associated with forest clearing and conversion to agriculture and pasture, which makes evapotranspiration far more seasonal [65–67].

The amplification measure considered here using ERA5 and station data could also be investigated in global climate model simulations. If climate models are able to accurately simulate observed regional variability in A , more confidence could be placed in their projections of future changes in A . It can be hypothesized that if global warming continues, the distribution of A will gradually shift over time as climate zones migrate [68,69] and moisture limitation of evaporation becomes more widespread in the tropics and temperate zones [70].

The comparison of temperature percentiles and their trends in ERA5 with station-based daily maximum temperature data showed substantial agreement between the reanalysis and station observation. Some discrepancies were identified, such as ERA5 having too little summer warming over the Great Lakes. These could be investigated further and hopefully corrected in future reanalysis versions.

5. Conclusions

It was found that over land, the maximum annual temperature tended to increase slightly more slowly than the 80th percentile maximum temperature, for a negative amplification (or dampening) of the hot temperature extremes. By contrast, over water, there was positive mean amplification. Specific continents and regions in the moist tropics and temperate mid-latitudes, such as much of Africa and Europe, showed positive amplification. Amplification could be affected by land-atmosphere feedbacks, including those associated with irrigated areas and with the physiological effects of rising CO_2 concentrations on plant transpiration, as well as with regional circulation and land use changes, which need to be investigated in more detail. These findings provide a new target for climate model calibration, and insight for evaluating the changing risk of temperature extremes.

Funding: This research was funded by the National Oceanic and Atmospheric Administration Educational Partnership Program with Minority-Serving Institutions—Cooperative Science Center for Earth System Sciences and Remote Sensing Technologies under the Cooperative Agreement Grant numbers NA16SEC4810008 and NA22SEC4810016. The statements contained within this article are not the opinions of the funding agency or the United States government but reflect the author’s opinions.

Data Availability Statement: The data used in this research is available to download from its respective providers.

Conflicts of Interest: The author declares no conflict of interest. The funders had no role in the design of the study; in the collection, analyses, or interpretation of data; in the writing of the manuscript, or in the decision to publish the results.

References

1. Tebaldi, C.; Hayhoe, K.; Arblaster, J.M.; Meehl, G.A. Going to the extremes. *Clim. Chang.* **2006**, *79*, 185–211. [[CrossRef](#)]
2. Alexander, L.V.; Zhang, X.; Peterson, T.C.; Caesar, J.; Gleason, B.; Klein Tank, A.M.G.; Haylock, M.; Collins, D.; Trewin, B.; Rahimzadeh, F.; et al. Global observed changes in daily climate extremes of temperature and precipitation. *J. Geophys. Res.* **2006**, *111*, D05109. [[CrossRef](#)]
3. McKinnon, K.A.; Rhines, A.; Tingley, M.P.; Huybers, P. The changing shape of Northern Hemisphere summer temperature distributions. *J. Geophys. Res. Atmos.* **2016**, *121*, 8849–8868. [[CrossRef](#)]
4. Tamarin-Brodsky, T.; Hodges, K.; Hoskins, B.J.; Shepherd, T.G. Changes in Northern Hemisphere temperature variability shaped by regional warming patterns. *Nat. Geosci.* **2020**, *13*, 414–421. [[CrossRef](#)]

5. Klein Tank, A.M.; Zwiers, F.W.; Zhang, X. *Guidelines on Analysis of Extremes in a Changing Climate in Support of Informed Decisions for Adaptation*; Technical Report; World Meteorological Organization: Geneva, Switzerland, 2009.
6. Zhang, X.; Alexander, L.; Hegerl, G.C.; Jones, P.; Tank, A.K.; Peterson, T.C.; Trewin, B.; Zwiers, F.W. Indices for monitoring changes in extremes based on daily temperature and precipitation data. *Wiley Interdiscip. Rev. Clim. Chang.* **2011**, *2*, 851–870. [[CrossRef](#)]
7. Seneviratne, S.I.; Zwiers, F.W. Attribution and prediction of extreme events: Editorial on the special issue. *Weather Clim. Extrem.* **2015**, *9*, 2–5. [[CrossRef](#)]
8. Easterling, D.R. Global Data Sets for Analysis of Climate Extremes. In *Extremes in a Changing Climate*; AghaKouchak, A., Easterling, D., Hsu, K., Schubert, S., Sorooshian, S., Springer: Dordrecht, The Netherlands, 2013; Volume 65, pp. 347–361. [[CrossRef](#)]
9. Coumou, D.; Robinson, A. Historic and future increase in the global land area affected by monthly heat extremes. *Environ. Res. Lett.* **2013**, *8*, 034018. [[CrossRef](#)]
10. Donat, M.G.; Alexander, L.V.; Yang, H.; Durre, I.; Vose, R.; Dunn, R.J.H.; Willett, K.M.; Aguilar, E.; Brunet, M.; Caesar, J.; et al. Updated analyses of temperature and precipitation extreme indices since the beginning of the twentieth century: The HadEX2 dataset. *J. Geophys. Res.* **2013**, *118*, 2098–2118. [[CrossRef](#)]
11. Milagros de los Skansi, M.; Brunet, M.; Sigro, J.; Aguilar, E.; Groening, J.A.A.; Bentancur, O.J.; Geier, Y.R.C.; Amaya, R.L.C.; Jácome, H.; Ramos, A.M.; et al. Warming and wetting signals emerging from analysis of changes in climate extreme indices over South America. *Glob. Planet. Chang.* **2013**, *100*, 295–307. [[CrossRef](#)]
12. Sillmann, J.; Kharin, V.V.; Zhang, X.; Zwiers, F.W.; Bronaugh, D. Climate extremes indices in the CMIP5 multi-model ensemble. Part 1: Model evaluation in the present climate. *J. Geophys. Res.* **2013**, *118*, 1716–1733. [[CrossRef](#)]
13. Mistry, M. A High-Resolution Global Gridded Historical Dataset of Climate Extreme Indices. *Data* **2019**, *4*, 41. [[CrossRef](#)]
14. Zaitchik, B.F.; Tuholske, C. Earth observations of extreme heat events: Leveraging current capabilities to enhance heat research and action. *Environ. Res. Lett.* **2021**, *16*, 111002. [[CrossRef](#)]
15. Mishra, V.; Ganguly, A.R.; Nijssen, B.; Lettenmaier, D.P. Changes in observed climate extremes in global urban areas. *Environ. Res. Lett.* **2015**, *10*, 024005. [[CrossRef](#)]
16. Habeeb, D.; Vargo, J.; Stone, B. Rising heat wave trends in large US cities. *Nat. Hazards* **2015**, *76*, 1651–1665. [[CrossRef](#)]
17. Stillman, J.H. Heat Waves, the New Normal: Summertime Temperature Extremes Will Impact Animals, Ecosystems, and Human Communities. *Physiology* **2019**, *34*, 86–100. [[CrossRef](#)]
18. Kennedy-Asser, A.T.; Andrews, O.; Mitchell, D.M.; Warren, R.F. Evaluating heat extremes in the UK Climate Projections (UKCP18). *Environ. Res. Lett.* **2020**, *16*, 014039. [[CrossRef](#)]
19. Mueller, N.D.; Butler, E.E.; McKinnon, K.A.; Rhines, A.; Tingley, M.; Holbrook, N.M.; Huybers, P. Cooling of US Midwest summer temperature extremes from cropland intensification. *Nat. Clim. Chang.* **2015**, *6*, 317–322. [[CrossRef](#)]
20. Thiery, W.; Visser, A.J.; Fischer, E.M.; Hauser, M.; Hirsch, A.L.; Lawrence, D.M.; Lejeune, Q.; Davin, E.L.; Seneviratne, S.I. Warming of hot extremes alleviated by expanding irrigation. *Nat. Commun.* **2020**, *11*, 290. [[CrossRef](#)]
21. Wu, X.; Wang, L.; Yao, R.; Luo, M.; Li, X. Identifying the dominant driving factors of heat waves in the North China Plain. *Atmos. Res.* **2021**, *252*, 105458. [[CrossRef](#)]
22. Oldenborgh, G.J.V.; Wehner, M.F.; Vautard, R.; Otto, F.E.L.; Seneviratne, S.I.; Stott, P.A.; Hegerl, G.C.; Philip, S.Y.; Kew, S.F. Attributing and Projecting Heatwaves Is Hard: We Can Do Better. *Earth's Future* **2022**, *10*, e2021EF002271. [[CrossRef](#)]
23. Seneviratne, S.I.; Zhang, X.; Adnan, M.; Badi, W.; Dereczynski, C.; Di Luca, A.; Ghosh, S.; Iskandar, I.; Kossin, J.; Lewis, S.; et al. Weather and climate extreme events in a changing climate. In *Climate Change 2021: The Physical Science Basis. Contribution of Working Group I to the Sixth Assessment Report of the Intergovernmental Panel on Climate Change*; Cambridge University Press: Cambridge, UK, 2021.
24. Di Luca, A.; de Elía, R.; Bador, M.; Argüeso, D. Contribution of mean climate to hot temperature extremes for present and future climates. *Weather Clim. Extrem.* **2020**, *28*, 100255. [[CrossRef](#)]
25. Di Luca, A.; Pitman, A.J.; de Elía, R. Decomposing Temperature Extremes Errors in CMIP5 and CMIP6 Models. *Geophys. Res. Lett.* **2020**, *47*, e2020GL088031. [[CrossRef](#)]
26. Krakauer, N.Y. Shifting hardiness zones: Trends in annual minimum temperature. *Climate* **2018**, *6*, 15. [[CrossRef](#)]
27. Dunn, R.J.H.; Willett, K.M.; Thorne, P.W.; Woolley, E.V.; Durre, I.; Dai, A.; Parker, D.E.; Vose, R.S. HadISD: A quality-controlled global synoptic report database for selected variables at long-term stations from 1973–2011. *Clim. Past* **2012**, *8*, 1649–1679. [[CrossRef](#)]
28. Dunn, R.J.H.; Willett, K.M.; Parker, D.E.; Mitchell, L. Expanding HadISD: Quality-controlled, sub-daily station data from 1931. *Geosci. Instrum. Methods Data Syst.* **2016**, *5*, 473–491. [[CrossRef](#)]
29. Hurvich, C.M.; Simonoff, J.S.; Tsai, C.L. Smoothing parameter selection in nonparametric regression using an improved Akaike information criterion. *J. R. Stat. Soc.* **1998**, *60B*, 271–293. [[CrossRef](#)]
30. Krakauer, N.Y. Estimating climate trends: Application to United States plant hardiness zones. *Adv. Meteorol.* **2012**, *2012*, 404876. [[CrossRef](#)]
31. ERA5 Reanalysis (0.25 Degree Latitude-Longitude Grid). 2019. Available online: <https://rda.ucar.edu/datasets/ds633.0/> (accessed on 3 January 2023). [[CrossRef](#)]

32. Hersbach, H.; de Rosnay, P.; Bell, B.; Schepers, D.; Simmons, A.; Soci, C.; Abdalla, S.; Alonso-Balmaseda, M.; Balsamo, G.; Bechtold, P.; et al. *Operational Global Reanalysis: Progress, Future Directions and Synergies with NWP*; Technical Report 27; ECMWF: London, UK, 2018. [[CrossRef](#)]
33. Domínguez-Castro, F.; Reig, F.; Vicente-Serrano, S.M.; Aguilar, E.; Peña-Angulo, D.; Noguera, I.; Revuelto, J.; van der Schrier, G.; El Kenawy, A.M. A multidecadal assessment of climate indices over Europe. *Sci. Data* **2020**, *7*, 125. Uses European Climate Assessment & Dataset (ECA&D) E-OBS gridded dataset and ERA5. [[CrossRef](#)] [[PubMed](#)]
34. Mishra, V.; Ambika, A.K.; Asoka, A.; Aadhar, S.; Buzan, J.; Kumar, R.; Huber, M. Moist heat stress extremes in India enhanced by irrigation. *Nat. Geosci.* **2020**, *13*, 722–728. [[CrossRef](#)]
35. Freychet, N.; Hegerl, G.; Mitchell, D.; Collins, M. Future changes in the frequency of temperature extremes may be underestimated in tropical and subtropical regions. *Commun. Earth Environ.* **2021**, *2*, 28. [[CrossRef](#)]
36. Li, X.X. Heat wave trends in Southeast Asia during 1979–2018: The impact of humidity. *Sci. Total Environ.* **2020**, *721*, 137664. [[CrossRef](#)]
37. Krakauer, N.Y.; Cook, B.I.; Puma, M.J. Effect of irrigation on humid heat extremes. *Environ. Res. Lett.* **2020**, *15*, 094010. [[CrossRef](#)]
38. Menne, M.; Durre, I.; Vose, R.; Gleason, B.; Houston, T. An overview of the Global Historical Climatology Network-Daily database. *J. Atmos. Ocean. Technol.* **2012**, *29*, 897–910. [[CrossRef](#)]
39. Jaffrés, J.B. GHCN-Daily: A treasure trove of climate data awaiting discovery. *Comput. Geosci.* **2019**, *122*, 35–44. [[CrossRef](#)]
40. Durre, I.; Menne, M.J.; Gleason, B.E.; Houston, T.G.; Vose, R.S. Comprehensive automated quality assurance of daily surface observations. *J. Appl. Meteorol. Climatol.* **2010**, *49*, 1615–1633. [[CrossRef](#)]
41. Doxsey-Whitfield, E.; MacManus, K.; Adamo, S.B.; Pistolesi, L.; Squires, J.; Borkovska, O.; Baptista, S.R. Taking Advantage of the Improved Availability of Census Data: A First Look at the Gridded Population of the World, Version 4. *Pap. Appl. Geogr.* **2015**, *1*, 226–234. [[CrossRef](#)]
42. Center For International Earth Science Information Network-CIESIN-Columbia University. *Gridded Population of the World, Version 4 (GPWv4): Population Count, Revision 11*; Columbia University: New York, NY, USA, 2018. . [[CrossRef](#)]
43. Siebert, S.; Döll, P.; Hoogeveen, J.; Faures, J.M.; Frenken, K.; Feick, S. Development and validation of the global map of irrigation areas. *Hydrol. Earth Syst. Sci.* **2005**, *9*, 535–547. [[CrossRef](#)]
44. Siebert, S.; Burke, J.; Faures, J.M.; Frenken, K.; Hoogeveen, J.; Döll, P.; Portmann, F.T. Groundwater use for irrigation—A global inventory. *Hydrol. Earth Syst. Sci.* **2010**, *14*, 1863–1880. [[CrossRef](#)]
45. Wilcox, R. A Note on the Theil-Sen Regression Estimator When the Regressor Is Random and the Error Term Is Heteroscedastic. *Biom. J.* **1998**, *40*, 261–268. [[CrossRef](#)]
46. Sen, P.K. Estimates of the regression coefficient based on Kendall’s tau. *J. Am. Stat. Assoc.* **1968**, *63*, 1379–1389. [[CrossRef](#)]
47. Chen, L.; Dirmeyer, P.A. Global observed and modelled impacts of irrigation on surface temperature. *Int. J. Climatol.* **2019**, *39*, 2587–2600. [[CrossRef](#)]
48. Albaladejo-García, J.A.; Alcon, F.; Martínez-Paz, J.M. The Irrigation Cooling Effect as a Climate Regulation Service of Agroecosystems. *Water* **2020**, *12*, 1553. [[CrossRef](#)]
49. Lebassi-Habtezion, B.; González, J.; Bornstein, R. Modeled large-scale warming impacts on summer California coastal-cooling trends. *J. Geophys. Res.* **2011**, *116*, D20114. [[CrossRef](#)]
50. Potter, C. Understanding climate change on the California coast: Accounting for extreme daily events among long-term trends. *Climate* **2014**, *2*, 18–27. [[CrossRef](#)]
51. Mason, L.A.; Riseng, C.M.; Gronewold, A.D.; Rutherford, E.S.; Wang, J.; Clites, A.; Smith, S.D.P.; McIntyre, P.B. Fine-scale spatial variation in ice cover and surface temperature trends across the surface of the Laurentian Great Lakes. *Clim. Chang.* **2016**, *138*, 71–83. [[CrossRef](#)]
52. Zhong, Y.; Notaro, M.; Vavrus, S.J. Spatially variable warming of the Laurentian Great Lakes: An interaction of bathymetry and climate. *Clim. Dyn.* **2018**, *52*, 5833–5848. [[CrossRef](#)]
53. White, C.; Heidinger, A.; Ackerman, S.; McIntyre, P. A Long-Term Fine-Resolution Record of AVHRR Surface Temperatures for the Laurentian Great Lakes. *Remote Sens.* **2018**, *10*, 1210. [[CrossRef](#)]
54. Alexander, L.; Perkins, S. Debate heating up over changes in climate variability. *Environ. Res. Lett.* **2013**, *8*, 041001. [[CrossRef](#)]
55. Byrne, M.P.; O’Gorman, P.A. Trends in continental temperature and humidity directly linked to ocean warming. *Proc. Natl. Acad. Sci. USA* **2018**, *115*, 4863–4868. [[CrossRef](#)]
56. Byrne, M.P. Amplified warming of extreme temperatures over tropical land. *Nature Geosci.* **2021**, *14*, 837–841. [[CrossRef](#)]
57. Fischer, E.M.; Seneviratne, S.I.; Vidale, P.L.; Luthi, D.; Schar, C. Soil moisture—Atmosphere interactions during the 2003 European summer heat wave. *J. Clim.* **2007**, *20*, 5081–5099. [[CrossRef](#)]
58. Zampieri, M.; D’Andrea, F.; Vautard, R.; Ciais, P.; de Noblet-Ducoudré, N.; Yiou, P. Hot European summers and the role of soil moisture in the propagation of Mediterranean drought. *J. Clim.* **2009**, *22*, 4747–4758. [[CrossRef](#)]
59. Stéfanon, M.; Drobinski, P.; D’Andrea, F.; Lebeaupin-Brossier, C.; Bastin, S. Soil moisture-temperature feedbacks at meso-scale during summer heat waves over Western Europe. *Clim. Dyn.* **2014**, *42*, 1309–1324. [[CrossRef](#)]
60. Lemordant, L.; Gentile, P. Vegetation Response to Rising CO2 Impacts Extreme Temperatures. *Geophys. Res. Lett.* **2018**, *46*, 1383–1392. Available online: <https://agupubs.onlinelibrary.wiley.com/doi/pdf/10.1029/2018GL080238> (accessed on 3 January 2023). [[CrossRef](#)]

61. Lobell, D.B.; Bonfils, C.J.; Kueppers, L.M.; Snyder, M.A. Irrigation cooling effect on temperature and heat index extremes. *Geophys. Res. Lett.* **2008**, *35*. [[CrossRef](#)]
62. Thiery, W.; Davin, E.L.; Lawrence, D.M.; Hirsch, A.L.; Hauser, M.; Seneviratne, S.I. Present-day irrigation mitigates heat extremes. *J. Geophys. Res. Atmos.* **2017**, *122*, 1403–1422. [[CrossRef](#)]
63. Xu, Y.; Lamarque, J.F.; Sanderson, B.M. The importance of aerosol scenarios in projections of future heat extremes. *Clim. Chang.* **2018**, *146*, 393–406. [[CrossRef](#)]
64. Hirschi, M.; Seneviratne, S.I.; Alexandrov, V.; Boberg, F.; Boroneant, C.; Christensen, O.B.; Formayer, H.; Orłowsky, B.; Stepanek, P. Observational evidence for soil-moisture impact on hot extremes in southeastern Europe. *Nat. Geosci.* **2011**, *4*, 17–21. [[CrossRef](#)]
65. Fan, Y.; Miguez-Macho, G. Potential groundwater contribution to Amazon evapotranspiration. *Hydrol. Earth Syst. Sci.* **2010**, *14*, 2039–2056. [[CrossRef](#)]
66. Markewitz, D.; Devine, S.; Davidson, E.A.; Brando, P.; Nepstad, D.C. Soil moisture depletion under simulated drought in the Amazon: impacts on deep root uptake. *New Phytol.* **2010**, *187*, 592–607. [[CrossRef](#)]
67. Swann, A.L.S.; Koven, C.D. A Direct Estimate of the Seasonal Cycle of Evapotranspiration over the Amazon Basin. *J. Hydrometeorol.* **2017**, *18*, 2173–2185. [[CrossRef](#)]
68. Beck, H.E.; Zimmermann, N.E.; McVicar, T.R.; Vergopolan, N.; Berg, A.; Wood, E.F. Present and future Köppen-Geiger climate classification maps at 1-km resolution. *Sci. Data* **2018**, *5*, 180214. [[CrossRef](#)] [[PubMed](#)]
69. Cui, D.; Liang, S.; Wang, D. Observed and projected changes in global climate zones based on Köppen climate classification. *WIREs Clim. Chang.* **2021**, *12*, e701. [[CrossRef](#)]
70. Dai, A. Increasing drought under global warming in observations and models. *Nat. Clim. Chang.* **2013**, *3*, 52–58. [[CrossRef](#)]

Disclaimer/Publisher’s Note: The statements, opinions and data contained in all publications are solely those of the individual author(s) and contributor(s) and not of MDPI and/or the editor(s). MDPI and/or the editor(s) disclaim responsibility for any injury to people or property resulting from any ideas, methods, instructions or products referred to in the content.